Device optimization of $CsSnI_{2.95}F_{0.05}$-based all-solid-state dye-sensitized solar cells with non-linear charge-carrier-density dependent photovoltaic behaviors

Shuai Ma[a], Mingwei Shang[a,b], Liyan Yu[a], and Lifeng Dong[a,b*]

[a] College of Materials Science and Engineering, Qingdao University of Science and Technology, Qingdao, 266042, P. R. China
[b] Department of Physics, Astronomy, and Materials Science, Missouri State University, Springfield, Missouri, 65897, USA (E-mail: donglifeng@qust.edu.cn)

Supporting Information

1. Experiments of material synthesis

TiO_2 nanorod array was deposited on FTO glass by a simple hydrothermal method, utilizing $Ti(OBu)_4$ as the titanium precursor and hydrochloric acid. The hydrothermal reaction was maintained at 155 °C for 4 h. Afterwards the as-deposited TiO_2 film was annealed at 450 °C for 3 h. The obtained TiO_2 electrodes were immersed in 0.3 mM ethanol solution of *cis*-diisothiocyanato-*bis*-(2,20-bipyridyl-4,40-dicaboxylato)-ruthenium(II)bis(tetrabutyl-ammonium) (N719, DYESOL) at room temperature for 18 h, then rinsed by ethanol to remove the unabsorbed dye molecule. Finally the dye-sensitized TiO_2 photoelectrode was obtained after air-dried.

Pt counter electrode was prepared by coating an FTO glass substrate with a thin layer of 5 mM H_2PtCl_6 solution in isopropanol and subsequently heating at 400 °C for 0.5 h.

2. Hysteresis test of $CsSnI_{2.95}F_{0.05}$-based solar cells

Hysteresis problem of $CsSnI_{2.95}F_{0.05}$-based solar cells can be verified by varying the biased voltage scan rate and orientation during the photovoltaic measurements. Specifically, j-V characteristics of our fabricated cells were acquired under AM1.5 100 mW/cm^2 sun simulator with a scan rate ranging from 0.001 to 0.15 V/s, as shown in fig.S1, of which 'LH(solid lines)' and 'HL(dash lines)' represents the forward and backward voltage scan orientation from 0 to -1V and from -1 to 0V, respectively.

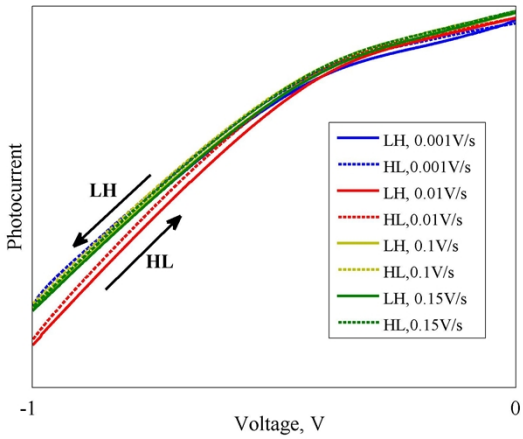

Fig.S1 Photovoltaic response for hysteresis test of our fabricated solar cells, characterizing at different scan rate at 0.001 V/s to 0.15 V/s with both forward/backward scan orientations.

We conclude that although $CsSnI_{2.95}F_{0.05}$ is perovskite semiconductor compound,[S1] our fabricated solar cells prove no such hysteresis phenomenon at whatever scan rate, even if we randomly chose the test cells without doing particular device optimization. And this experimental result is quite consistent to H. J. Snaith's discovery [S2] on the correlation between the hysteresis and thickness of mesoporous TiO_2 layer.

3. EQE measurement system

EQE spectra were acquired by using a measurement system (shown in fig.S2) composed of a xenon lamp as simulated light source (Model 66902, Newport), a filter (Model 74010, Newport) coupled with a monochromator (Model 74125, Newport), a lock-in amplifier (Model 70104 Merlin, Newport), and a standard silicon photodiode (Model 70356,

Newport) as calibration unit. EQE measurements were typically done by scanning the wavelength from 400 to 800 nm with around 10 nm wavelength intervals. The measurement was implemented at AC mode, and the exported light intensity roughly approximated to 0.1 mW/cm^2.

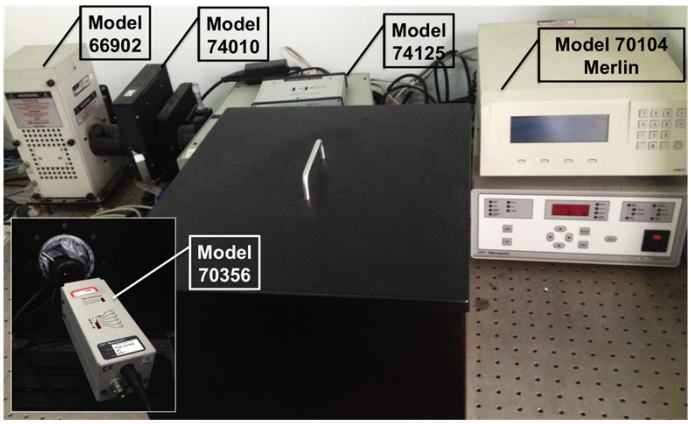

Fig.S2 The measurement system used for EQE analysis.

4. Photoelectric characterization of the optimized $CsSnI_{2.95}F_{0.05}$-based all-solid-state DSCs:

Statistic diagram fig.S3(a) of 19 samples fabricated on the same condition after electrolyte precursor injected for 48 h and measured under 14.2 mW/cm^2 illumination. It turns out that the average PCE is around 7.7% and the best efficiency reaches up to 9.8%. And fig.S3(b) gives a typical *j-V* characteristics with PCE~7.7% under 14.2 mW/cm^2.

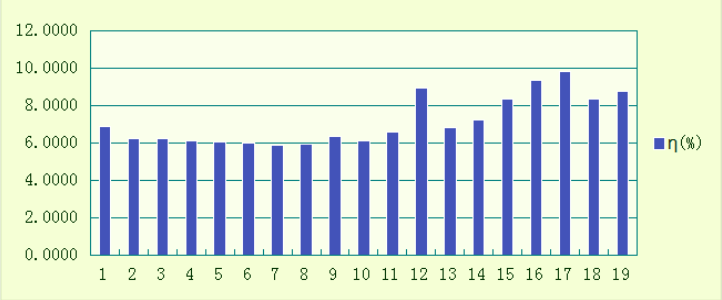

(a)

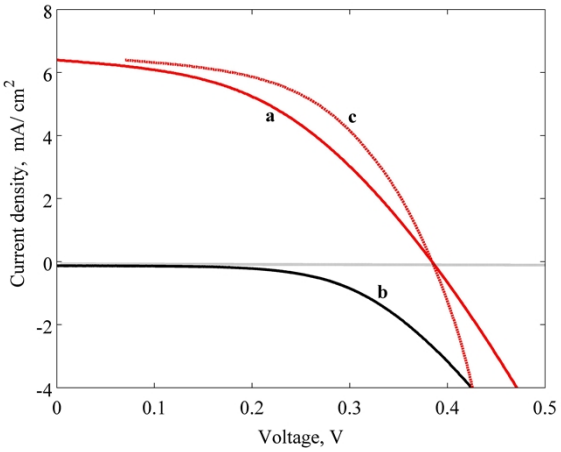

(b)

Fig. S3 (a) Statistic diagram of power conversion efficiency distribution of 19 solar cells after the electrolyte precursor injected for 48 h. (b) *j-V* characteristics of one of 19 solar cells. a: light state with $\eta \approx 7.7\%$, *FF*=0.44 @14.2 mW/cm^2, b: dark state, c: *j-V* by excluding series resistance R_s (~10 Ω cm^2) from entire circuit.

5. Transport parameters extraction from EIS and OCVD measurements

EIS measurement corresponding to the solar cell used in *j-V* characterization of fig.1. Unlike the Nyquist plot of conventional DSCs, the coexistent two arcs can be observed in that of SDSCs sometimes (fig.S4), so we have to implement the study on corresponding two processes, *i.e.*, carrier transport properties (with impedance Z_h) through HTM and interfacial process (Z_{ct}) at the $TiO_2/CsSnI_{2.95}F_{0.05}$ junction. For the DSCs with a liquid electrolyte, impedance associating to electrolyte is usually identified from the EIS pattern as an arc appearing in frequency regions lower than that of Z_{ct}; instead, regarding to the solid-state electrolyte employed, a characteristic arc at higher frequencies is observed in the impedance spectra. This characteristic frequency range has also been demonstrated by EIS of other kind of solar cells that adopt solid-state hole transport materials[S3,S4]. And by chance Z_h can even transform into a straight tilted lines from the magnified Nyquist plots, just similar to the EIS observation on other kind of solid-state nanostructure solar cells [S3].

Specifically, the semi-circle in low frequency range usually represents interfacial properties of Z_{ct}, which has a quite mature equivalent circuit called transmission-line (TL) model[S5,S6] to describe it. But during experimental observations, some EIS spectrum only has one deformed big arc, and that is constructed by merging of Z_h and Z_{ct} together, since sometimes these two characteristic frequencies are quite closed to each other.

The solid curves accompanying measured Nyquist plots are generated from fitting based on the equivalent circuit model proposed by fig. S4 and the fitting quality is generally good. Specifically, according to this circuit model, R_s represents the series resistance of the circuit; sintered nanoporous TiO_2 film is modeled by TL model we have already mentioned, which generally describes electron transport channel throughout TiO_2 film and involves corresponding transport resistance (R_t) as well as TiO_2/HTM interfacial property Z_{ct}; for Z_h it is basically equivalent to another resistance-capacitance circuit block as we used R_h-C_h in paralleled; the paralleled R_{ce} and C_{ce} are related to the charge transfer occurred at interface of counter-electrode, though in practical measurement this block is almost invisible in our case.

The previous work has demonstrated that circuit elements are directly linked to the small-signal transport and recombination parameters, according to eq.(S1-S3). Thus the effective lifetime, diffusivity and diffusion length of electrons can be computed in this way.

$$\tau_{eff} = R_{ct} C_{\mu} \tag{S1}$$

$$D_n = \frac{d^2}{R_t C_{\mu}} \tag{S2}$$

$$L_n = d\sqrt{\frac{R_{ct}}{R_t}} \tag{S3}$$

According to the analysis on fig.S5(a), *i.e.* the Nyquist plots measured under illumination condition (1 sun) at different voltage bias ranging from 0.1 to 0.6V, three critical small-signal parameters including diffusion length, effective lifetime and diffusivity have been extracted based on equivalent circuit fitting method. It is observed from fig.S5(b) that L_n slightly decreases with bias voltage and the average magnitude around 5-6 μm, which is much higher than the thickness of active layer and thus guarantee the sufficient charge carrier collection efficiency[S7]. Instead, τ_{eff} and D_n exhibit the obvious tendency along with biased potential increasing, especially in the range from knee voltage to open-circuit voltage.

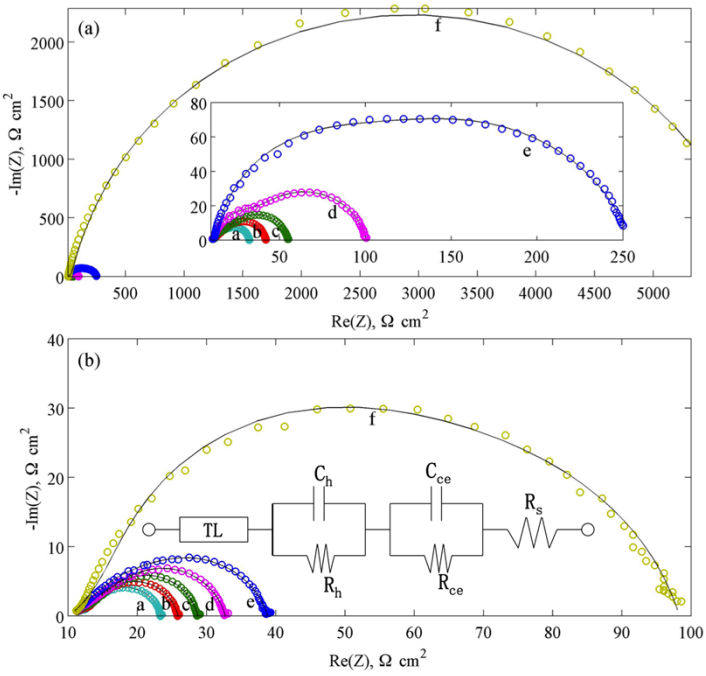

Fig.S4 Nyquist plots of solar cell with electrolyte precursor soaking onto TiO_2 electrode for 48 h. The cell was biased under 14.2 mW/cm2 illumination condition at a-0.484 V, b-0.434 V, c-0.384 V, d-0.334 V, e-0.284 V, f-0.124 V.

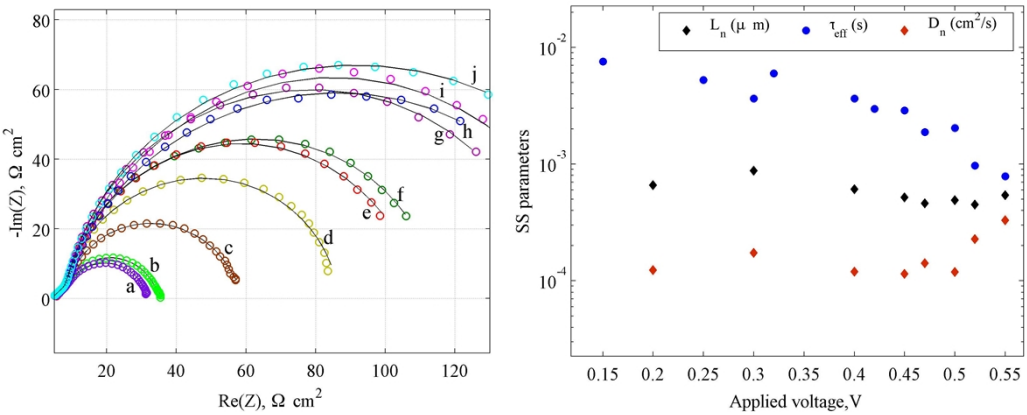

Fig.S5 (a) Nyquist plots measured under illumination condition (1 sun) at different voltage bias (circle plots): a-0.6V, b-0.57V, c-0.55V, d-0.5V, e-0.47V, f-0.45V, g-0.4V, h-0.3V, i-0.2V, j-0.1V. The solid lines represent the fitting results. (b) The extracted small-signal parameters, *i.e.* diffusion length L_n, effective lifetime and diffusivity, varying with bias voltage.

OCVD has certain advantages over other frequency or steady-state-based methods: it provides a continuous reading of the lifetime as a function of V_{oc} with high voltage resolution; besides, the experimental realization and corresponding data treatment are quite simple for obtaining valuable information of recombination mechanisms.

OCVD conducts a quasi-equilibrium measurement that monitors the subsequent photovoltage decay when switching the cell operation from light to dark condition. Its experimental realization can be facilely achieved that just needs the excitation contributed by a continuous light source for forward biasing the solar cell.[S8] The data treatment for extracting the information on the recombination mechanisms is also relatively simple, compared to that of other frequency or steady-state-based techniques. The response time can be computed by the reciprocal of the derivative of the decay curve normalized by the thermal voltage:

$$\tau_{eff} = \frac{k_B T}{q}\left|\frac{1}{\mathrm{d}V_{oc}/\mathrm{d}t}\right| \tag{S4}$$

6. Optical model coupled in device-level modeling:

For the developed solar cell with stack structure, the optical model is supposed to consider every process associating to irradiation absorption and energy losses occurring as the light passes through each layer, due to the reflection or the incomplete transmission coming from substrate glass or photoelectrode itself. For the sake of simplicity, only the perpendicular photon flux with respect to the cell interfaces is taken into consideration in modeling. The optical generation rate G_{op} with sun illumination injecting from photoelectrode is written as:

$$G_{op} = \int_{\lambda} \Phi(\lambda)\,\eta_{ill}(\lambda)\,\alpha_{dye}(\lambda)\,\mathrm{e}^{-\alpha(\lambda)x}\mathrm{d}\lambda \tag{S5}$$

where Φ represents the total spectral solar photon flux density (with unit $cm^{-2}s^{-1}\mu m^{-1}$), and it is evaluated from a specific air mass solar irradiation power density P ($Wcm^{-2}\mu m^{-1}$), e.g. under the AM1.5g as $\Phi=(P\lambda)/(1.24q)$. η_{ill} represents the illumination efficiency by excluding the optical losses from transmission and reflection, *i.e.* $\eta_{ill}(\lambda)=T(\lambda)[1-R(\lambda)]$, in which $T(\lambda)$ and $R(\lambda)$ represent the transmittance of FTO substrate and reflectance of photoelectrode, respectively. Besides, we assume the total absorption coefficient α_{abs} approximated to be summary of α_{dye} and α_{TiO2}, whereas temporarily ignore the absorption contributed by $CsSnI_{2.95}F_{0.05}$. The correlative optical parameters employed in calculation are shown in fig.S6, which come from the data of authors' previous work about conventional DSCs[S9]; meanwhile, the peak values of them have been slightly tuned in order to match our current measurement data.

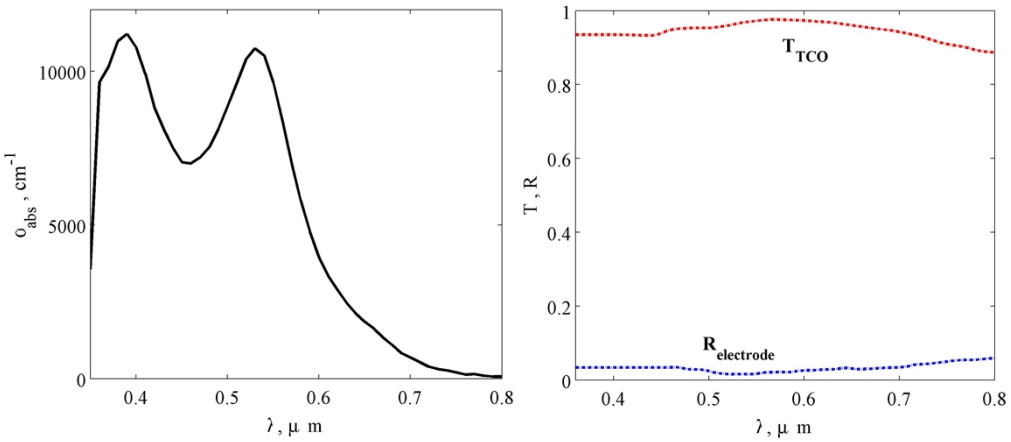

Fig. S6 The total absorption coefficient α_{abs}; the transmittance and reflectance associating to the FTO substrate and working electrode.

7. Trap distribution factor α_T:

Trap distribution factor α_T is possible to be precisely extracted from chemical capacitance C_μ vs.V relation since C_μ directly involves in trap carrier distribution. In general, chemical capacitance could be defined as:[S10]

$$C_\mu = dq\frac{\partial n}{\partial V} = \left(\frac{dq}{V_T}n_0\right)e^{V/V_T} \tag{S6}$$

In fact, practically the trap would always dominate in TiO_2 nanoporous film, according to which the expression of C_μ has to be redefined as:

$$C_\mu^T = dq\frac{\partial n_t}{\partial V} = \left(\frac{dq}{V_T}\alpha_T N_T\right)\left(\frac{n_0}{N_c}\right)^{\alpha_T} e^{\alpha_T\frac{V}{V_T}} \tag{S7}$$

Consequently, chemical capacitance obtained from EIS measurement exactly obeys the exponential relation with respect to biased voltage. According to $\ln(C_\mu)\sim(\alpha_T/V_T)\ V$ of fig.S7, α_T derived from the exponent is around 0.1.

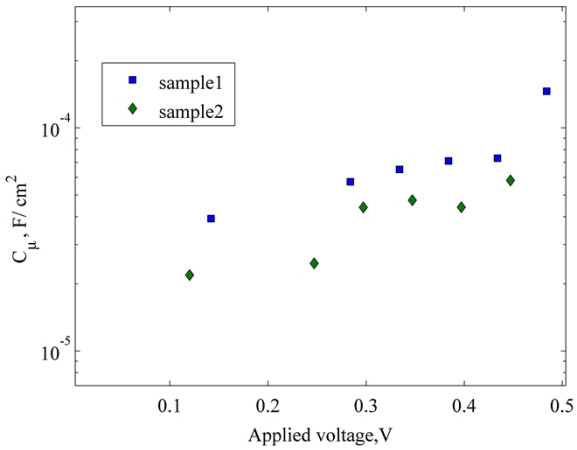

Fig.S7 Extracted C_μ-V from EIS measurements of two samples under 14.2 mW/cm^2 illumination, fitting by the relation of $\ln(C_\mu)\sim(\alpha_T/V_T)\ V$ and obtain α_T.

8. The influence of electrolyte precursor soaking time t_s

1) Fig. S8(a) shows the microscopic morphology of pure TiO_2 nanorod array, the pore distribution of which is quite uniform. The direct influence of electrolyte soaking time on morphology of TiO_2 nanorod array can be also observed, according to the microscopic morphology of fabricated electrodes with $CsSnI_{2.95}F_{0.05}$ soaking for 3 and 48 h as fig.S8(b).

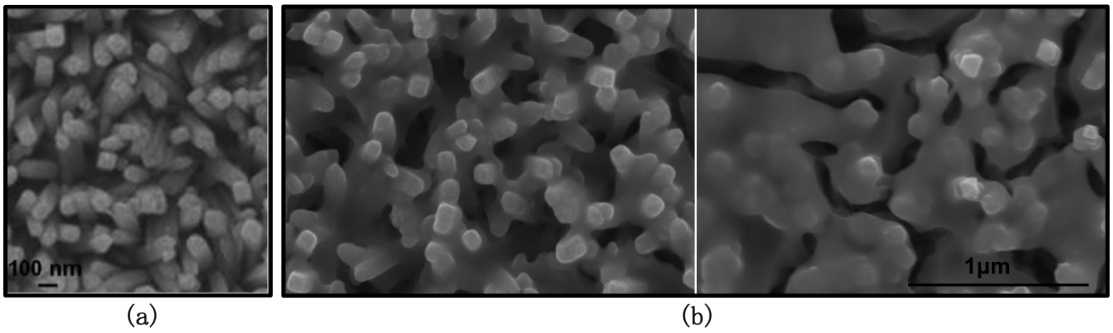

Fig.S8 (a) SEM photograph of pure TiO_2 nanorod array; (b) SEM photographs of $CsSnI_{2.95}F_{0.05}$ precursor on TiO_2 nanorod soaking for 3 h (left) and 48 h (right), respectively.

2) We measure voltage decay with respect to time under open-circuit condition (fig.S9a), and extract the effective lifetime of charge carriers with different electrolyte soaking time (fig.S9b). The apparent improvement of lifetime along with t_s increasing can be clearly observed especially at low potential (insert of fig.S9b); at higher potential instead, the discrepancy is negligible whatever t_s increasing. Since OCVD primarily considers the recombination between TiO_2 conduction band and hole transport materials as the EHR channel shown in schematic fig.1(b) of the manuscript, we have reason to believe that the promotion for the effective lifetime varying with respect to t_s could be more remarkable if other recombination mechanisms were considered simultaneously.

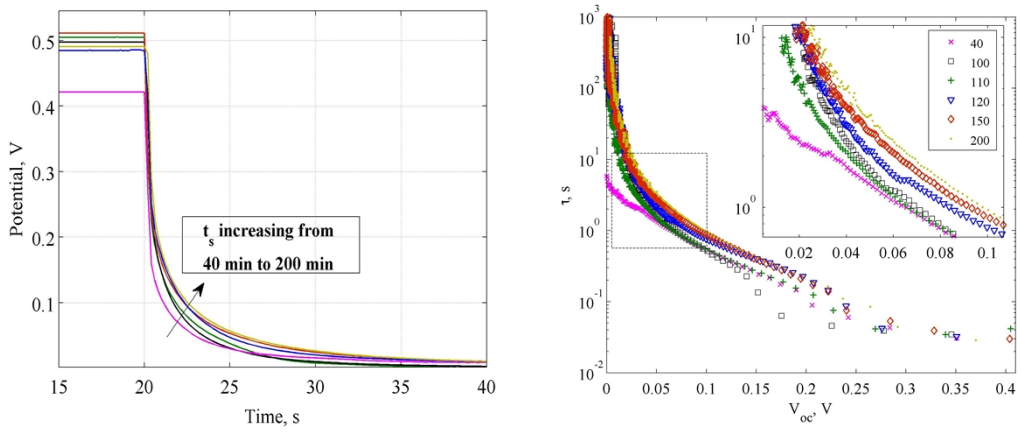

(a) (b)

Fig.S9 (a) The voltage decay at open-circuit condition for solid-state DSCs with different electrolyte soaking time t_s. (b) According to OCVD measurement, the extracted effective lifetime is indeed improved along with t_s increasing, especially within the first three hours (as labeled by the figure legend, from 40 to 200 min).

3) We repeated to fabricate a large group of solid-state DSCs with the same cell structure, only changing electrolyte precursor solution soaking time t_s. As shown in fig.S10, in general the primary peak of a group of EQE spectra was at 0.54 μm; along with ts increasing, the width of spectra also get apparent enlargement.

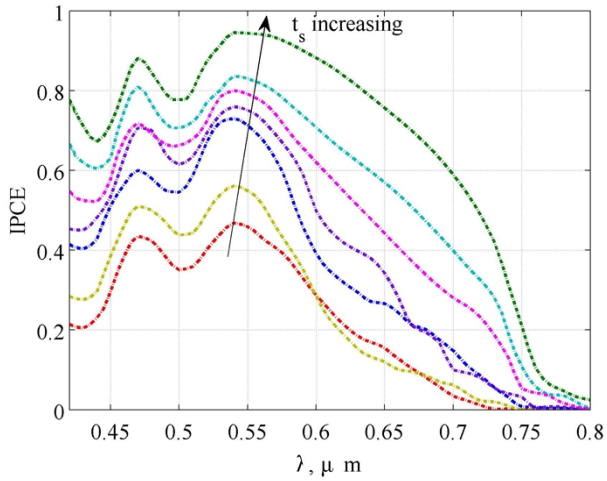

Fig.S10 Measured EQE spectra of solid-state DSCs with different electrolyte precursor soaking time t_s.

9. Photocurrent prediction according to EQE sepctra

Further, by integrating EQE spectrum of fig.S10 through visible light wavelength range according to equation (S8) below ([fig.S11(left)] shows the specific air mass solar irradiation power density used for integration), it allows us to simply predict the photocurrent. Then, by comparing the integrated value j_{integ} to j_{ph} from normal j-V measurements [fig.S11(right)], EQE measurements also prove clear tendency that j_{integ} increases with respect to t_s. On the other hand, according to the analysis of fig.7 in the manuscript, average charge collection efficiency $\overline{\eta}_{coll}$ illuminated by extremely low-intensity light should approximately be 30% higher than that under normal 1 sun illumination, and we expect that the similar difference between j_{integ} and j_{ph}, as long as EQE and j-V measurement systems have exactly the same electronic and optical loss apart from charge collection process. In practice according to fig.7, j_{integ} were only up to 10% higher than j_{ph}, probably because that we cannot guarantee to eliminate the discrepancy between two independent measurement systems.

$$j_{\text{integ}} = q\int \text{IPCE}(\lambda)\cdot\Phi_{\text{AM1.5}}(\lambda)\ \text{d}\lambda \tag{S8}$$

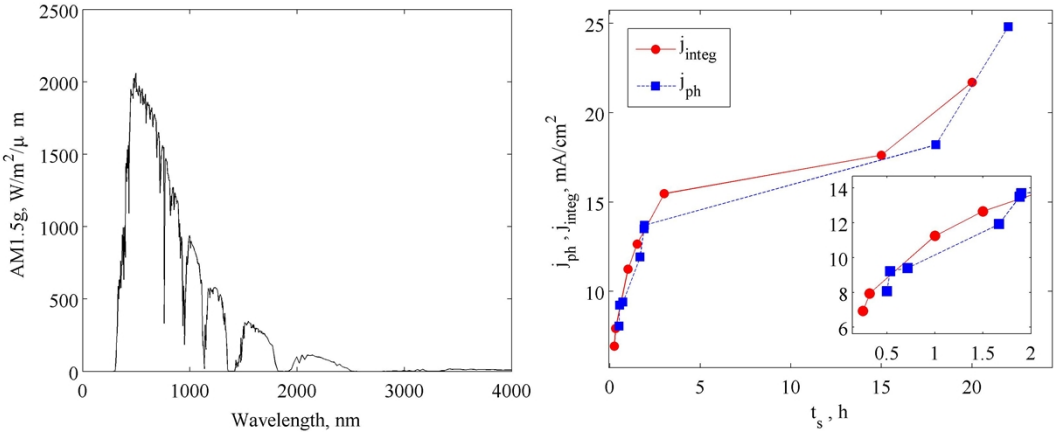

Fig.S11 (Left) Specific air mass solar irradiation power density [$Wcm^{-2}\mu m^{-1}$] used for integration by equation (S8); (Right) The comparison between j_{integ} and j_{ph} along with t_s increasing.

Reference

[S1] I. Borriello, G. Cantele, and D. Ninno. *Phys.Rev.B*,2008, **77**, 235214.
[S2] H. J. Snaith, A. Abate, J. M. Ball, *J. Phys. Chem. Lett.* 2014, **5**, 1511.
[S3] I. Mora-Sero, S. Gimenez, F. Fabregat-Santiago, etc. *Phys. Chem. Chem. Phys.,* 2011,**13,** 7162.
[S4] A. Dualeh, T. Moehl, M. K. Nazeeruddin, etc. *ACS Nano,* 2013,**7(3)**, 2292.
[S5] J. Bisquert, *Phys. Chem. Chem. Phys.,* 2000, **2,** 4185.
[S6] F. Fabregat-Santiago, J. Bisquert, G. Garcia-Belmonte, etc. *Sol. Energy Mater. Sol. Cells,* 2005, **87,** 117.
[S7] P.Docampo, A.Ivaturi, R.Gunning, etc. *J.Mater.Chem.A*, 2013, DOI: 10.1039/C3TA11855J.
[S8] C. J. Bruno, M. G. M. Bogado, J. C. Pla, etc. *Phys. Stat. Sol. (a)*, 1999, **174**, 231.
[S9] F. Cappelluti, S. Ma, D. Pugliese, etc. *Phys. Chem. Chem. Phys.*, 2013, **15**, 14634.
[S10] J. Bisquert. *Phys. Chem. Chem. Phys.*, 2003, **5**, 5360.